RSC Advances

PAPER

View Article Online
View Journal | View Issue

Cite this: *RSC Adv.*, 2024, **14**, 35498

Superior low temperature activity over α-MnO_2/β-MnOOH catalyst for selective catalytic reduction of NO_x with ammonia†

Masanori Takemoto, [a] Haruko Fujinuma,[a] Yoshihiro Sugawara,[b] Yukichi Sasaki,[b] Kenta Iyoki, [a] Tatsuya Okubo, [a] Kazuya Yamaguchi [c] and Toru Wakihara [ad]*

Manganese octahedral molecular sieves with an α-MnO_2 crystal structure (OMS-2) and their related materials have attracted significant attention for the selective catalytic reduction of NO_x using NH_3 (NH_3-SCR) at low temperatures. Further lowering their operating temperature should be an effective method to develop an environmentally friendly de-NO_x system; however, their catalytic activity at low temperatures, especially below 100 °C, remains poor. This study describes a post-synthetic approach to develop Mn-based catalysts superior to those in the literature that operate at ultralow temperatures. Post-synthetic planetary ball milling for OMS-2 caused the partial conversion of OMS-2 into β-MnOOH. The obtained nanocomposite catalysts possessed abundant surface oxygen vacancies and strong surface acidity, allowing the milled catalyst to exhibit higher NO conversion at 90 °C (91%) than that in freshly prepared OMS-2 without planetary ball milling (29%). Lowering the operation temperature of OMS-2 catalysts contributed to the suppression of N_2O evolution during NH_3-SCR over manganese-based catalysts, resulting in high N_2 selectivity over the milled OMS-2 catalyst (93%).

Received 16th August 2024
Accepted 24th October 2024

DOI: 10.1039/d4ra05934d

rsc.li/rsc-advances

Introduction

Removal of harmful NO_x is a critical process in industrial facilities such as thermal power stations and water-treatment plants because NO_x causes acid rain, ozone depletion, and photochemical smog.[1,2] Selective catalytic reduction of NO_x with NH_3 (NH_3-SCR: $4NH_3 + 4NO + O_2 \rightarrow 4N_2 + 6H_2O$) is one of the main methods to reduce NO_x.[3,4] In a stationary system to reduce NO_x, because exhaust gas also contains soot and SO_2 species, SCR catalysts should be located behind the particle elimination and desulfurization configurations to avoid deactivation from ash and SO_2.[5] Passing through the apparatus decreases the temperature of the exhaust gas. Among various catalysts, V_2O_5–WO_3/TiO_2,[6,7] V_2O_5–MoO_3/TiO_2,[8] and Cu-exchanged zeolite (SSZ-13)[4,9–12] have been widely accepted as suitable catalysts for practical use; however, their working temperatures are above 200 °C. Therefore, additional heat energy is required to activate vanadium-based and zeolite catalysts.

Manganese oxide is a popular catalyst attracting attention for environmental applications such as the catalytic decomposition of NO_x[13–16] and volatile organic compounds (VOCs),[17–22] owing to its large storage capacity, low cost, excellent redox properties, and variable valence states. Recently, manganese oxide catalysts have been considered as de-NO_x catalysts that work below 200 °C owing to their excellent redox properties and strong acidity. The different crystal structures of manganese oxides are α-, β-, γ-, θ-, and δ-, and previous studies have reported that α-MnO_2, denoted as OMS-2, exhibited especially higher catalytic activity for NH_3-SCR at low temperatures than that in MnO_2 with other crystal structures.[23,24] However, large amounts of N_2O, a greenhouse gas, are generally produced during the NH_3-SCR reaction,[16,25,26] which is the main barrier to the commercial utilization of manganese oxide catalysts. According to the literature, the formation rates of undesirable N_2O increase as temperatures increase.[16,25] Therefore, further lowering the operating temperatures of manganese oxide catalysts should be an effective strategy in the development of an environmentally friendly de-NO_x system. Although several techniques for enhancing the catalytic activity of OMS-2 at low temperatures have been investigated,[25,27–31] their catalytic activities remain unsatisfactory.

Post-synthesis treatment is a major strategy for tuning the chemical and physical properties of heterogeneous catalysts. Ball milling is well known as a technique for improving the

[a]*Department of Chemical System Engineering, School of Engineering, The University of Tokyo, 7-3-1 Hongo, Bunkyo-ku, Tokyo 113-8656, Japan. E-mail: wakihara@chemsys.t.u-tokyo.ac.jp*

[b]*Nanostructures Research Laboratory, Japan Fine Ceramics Center, 2-4-1 Mutsuno, Atsuta-ku, Nagoya 456-8587, Japan*

[c]*Department of Applied Chemistry, School of Engineering, The University of Tokyo, 7-3-1 Hongo, Bunkyo-ku, Tokyo 113-8656, Japan*

[d]*Institute of Engineering Innovation, The University of Tokyo, 2-11-16 Yayoi, Bunkyo-ku, Tokyo 113-8656, Japan*

† Electronic supplementary information (ESI) available. See DOI: https://doi.org/10.1039/d4ra05934d

activity of heterogeneous catalysts by controlling their size and morphology,[32] surface modification,[33] and defect-engineering.[34] Defect-rich surface structures have been proposed as preferable for enhancing the activity of Mn-based catalysts in NH_3-SCR.[31] Therefore, focusing on the possibility of introducing defect structures, post-synthesis ball milling has substantial potential for the enhancement of catalytic activity over OMS-2 catalysts at low temperatures.

This study demonstrates that the use of planetary ball milling as a post-synthetic treatment for OMS-2 allows to yield a de-NO_x catalyst operating at low temperatures that is superior to those in the literature. Starting from $KMnO_4$ and $MnSO_4 \cdot H_2O$, OMS-2 was prepared *via* a redox reaction in an acidic condition and followed by planetary ball milling at 400 rpm for different durations for OMS-2. This protocol allowed to yield nanocomposites of α-MnO_2/β-MnOOH with more abundant oxygen vacancies and stronger acid strengths than before milling. Such features contributed to the higher NO conversion over a nanocomposite catalyst at less than 150 °C than that over freshly prepared OMS-2 without planetary ball milling, which also contributed to the suppression of undesirable N_2O formation during low-temperature NH_3-SCR.

Experimental section

Catalyst preparation

Synthesis of OMS-2. OMS-2 was prepared as described previously.[35] 5.89 g $KMnO_4$ (FUJIFILM Wako Pure Chemical Corporation) was dissolved in 100 mL ultrapure water. The aqueous solution of $KMnO_4$ was added to an aqueous solution (30 mL) containing 8.8 g $MnSO_4 \cdot H_2O$ (Sigma-Aldrich) and 3 mL concentrated HNO_3 (FUJIFILM Wako Pure Chemical Corporation) in a round-bottle flask. The mixture was refluxed at 100 °C for 24 h in an oil bath. The resultant dark brown solid was filtered, washed with a large amount of water, and dried under air at 120 °C overnight. Hereafter, the obtained sample was named as "as-synthesize OMS-2".

Planetary ball milling for OMS-2. The milled samples were prepared by mechanically grinding of OMS-2 by using a planetary ball mill (Fritsch P6) equipped with silicon nitride balls and pot (Si_3N_4) ceramics sintered with Y_2O_3 and Al_2O_3 as additives. Milling was conducted using repeated rotation speed at 400 rpm for 5 min at 10 min intervals to avoid overheating the apparatus and reagents. The total milling time varied from 15 to 95 min (excluding the break time). The milled samples were recovered by water and dried at 80 °C overnight.

Characterization

Powder X-ray diffraction (PXRD) patterns of the samples were collected on a Rigaku Ultima IV instrument using Cu Kα radiation ($\lambda = 0.15406$ nm, 40 kV, 40 mA). Diffraction patterns were recorded in the angle range of $2\theta = 5$–70° with a scan speed of 0.1° min^{-1}. Nitrogen adsorption–desorption isotherms at −196 °C were obtained using a volumetric gas adsorption apparatus (NOVAtouch, Anton Paar). Before the measurements, sample powders were pretreated at 150 °C under a vacuum condition for 4 h. The specific surface area (S_{BET}) was estimated using the Brunauer–Emmett–Teller (BET) method. The morphologies of the samples were investigated using a field-emission scanning electron microscope (FE-SEM; JSM-IT800, JEOL) and a transmission electron microscope (TEM; JEM-F200, JEOL). The acidity and reducibility of the samples were examined using temperature-programmed desorption of NH_3 (NH_3-TPD) and temperature-programmed reduction of H_2 (H_2-TPR), respectively. NH_3-TPD and H_2-TPR profiles were recorded on a BELCAT II instrument (MicrotracBEL Corp.) using a thermal conductivity detector. For NH_3-TPD measurements, the samples (50 mg) were pretreated at 400 °C in He (50 sccm), and adsorbed 5.19% NH_3/He (50 sccm) at 50 °C for 30 min. He was passed through the reactor for another 15 min. Desorption was carried out under He flow (30 sccm) by increasing the temperature up to 500 °C at a rate of 10 °C min^{-1}. For H_2-TPR measurements, the samples (10 mg) were placed in the reactor, and the reactor was heated from room temperature to 700 °C with a heating rate of 10 °C min^{-1} in a reducing atmosphere of 5.03% H_2/Ar (30 sccm). X-ray photoelectron spectroscopy (XPS) spectra were recorded by using X-ray photoelectron spectrometer (JPS-9030, JEOL) under Al Kα radiation. The reference of XPS binding energy position was C 1s (284.2 eV) peak for all scans.

Catalytic measurement

The NH_3-SCR activity was conducted in a fixed-bed reactor operating at 60–240 °C. The concentrations of NO_x (sum of NO and NO_2), N_2O, and NH_3 in the outlet gas were determined using a chemiluminescence NO_x analyzer (ECL-88A Lite, Anatec Yanaco), gas chromatograph (GC-8A, Shimadzu), and gas analyzer (LGD F200P2-H NH_3, Axetris), respectively. An inlet gas containing 300 ppm NO, 300 ppm NH_3, 5% O_2, and balanced N_2 at a flow rate of 100 cm^3 min^{-1} was introduced to 50 mg of the catalyst. The following equation was used to calculate the NO conversion rate:

$$\text{NO conversion}(\%) = \frac{[NO_x]_{inlet} - [NO_x]_{outlet}}{[NO_x]_{inlet}} \times 100$$

The calculation equation of N_2 selectivity

$$= \frac{[NO_x]_{inlet} + [NH_3]_{inlet} - [NO_x]_{outlet} - [NH_3]_{outlet} - 2[N_2O]_{outlet}}{[NO_x]_{inlet} + [NH_3]_{inlet} - [NO_x]_{outlet} - [NH_3]_{outlet}} \times 100$$

Results and discussion

Preparation of catalysts

Fig. 1 shows the PXRD patterns of as-synthesized and milled OMS-2 catalysts. The diffraction peaks of as-synthesized OMS-2 correspond to those of α-MnO_2 (COD 9016667). The peak intensities decreased, and the diffraction peaks broadened in all diffraction patterns of the milled OMS-2, indicating the partial collapse/distortion of the original crystal structure. In

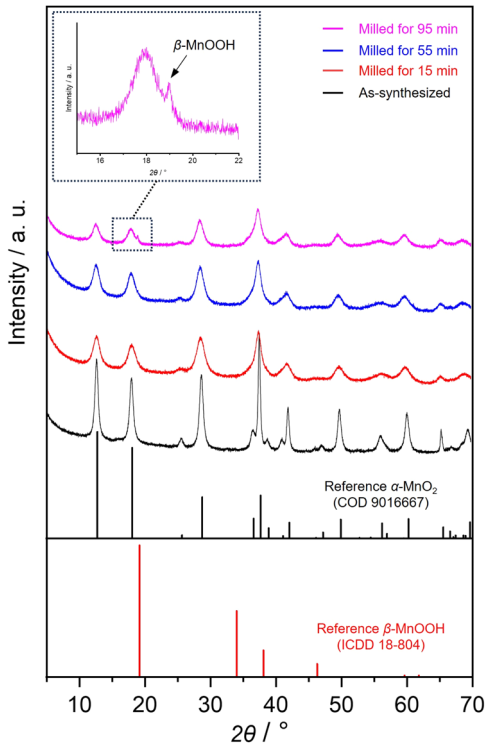

Fig. 1 PXRD patterns of as-synthesized and milled OMS-2 for different periods. Black arrow at 19.1° indicates a 00*l* reflection of feitknechtite, β-MnOOH.

the diffraction pattern of milled OMS-2 for 95 min, a sharp peak was also observed at 19.1° as highlighted by an arrow, which corresponds to a 00*l* reflection of feitknechtite, β-MnOOH.[36] This suggests that a part of α-MnO_2 was converted into β-MnOOH by the post-synthetic treatment.

The specific surface areas, SEM images and TEM images of as-synthesized and milled OMS-2 catalysts are summarized in Fig. 2. As-synthesized OMS-2 exhibited a high specific surface area of 65 m^2 g^{-1} and possessed rod-like morphology with a high aspect ratio (Fig. 2(a) and (b)), and these results are consistent with those in the literature.[17,35] Planetary ball milling treatment for 15 min induced the collapse of rod-like morphology followed by the formation of coarse aggregates composed of spherical particles (Fig. 2(c) and (d)), decreasing specific surface area (S_{BET} = 26 m^2 g^{-1}). Planetary ball milling treatments for 55 and 95 min caused growth of the thin-layered components (Fig. 2(e)–(h)). When comparing SEM images of milled samples for 55 and 95 min, long milling time induced the further growth of thin-layered components. Such thin-layered components would be presumably feitknechtite observed in X-ray diffraction (Fig. 1). The crystal structure of feitknechtite also predicted that the thin-layered components was feitknechtite (Fig. S1†). In particular, milled OMS-2 for 55 min certainly contained a tiny amount of feitknechtite which cannot be observed in XRD. Because of the formation of thin-layered components, milled OMS-2 for 55 and 95 min exhibited higher specific surface areas (S_{BET} = 67 and 70 m^2 g^{-1}) than its counterpart milled for 15 min. It can be summarized that planetary ball milling treatment for OMS-2 allowed to form nanocomposites of OMS-2 and feitknechtite with high specific surface areas.

Catalytic properties of catalysts

Fig. 3 shows NO conversion during NH_3-SCR over as-synthesized and milled OMS-2 catalysts. As-synthesized OMS-2 exhibited low NO conversion at 60 °C (8.7%). With the increase in reaction temperatures, NO conversion gradually increased and leached to 100% at 150 °C. 100% of NO conversion was maintained in the region of 150–210 °C. Milled OMS-2 for 15 min exhibited poor

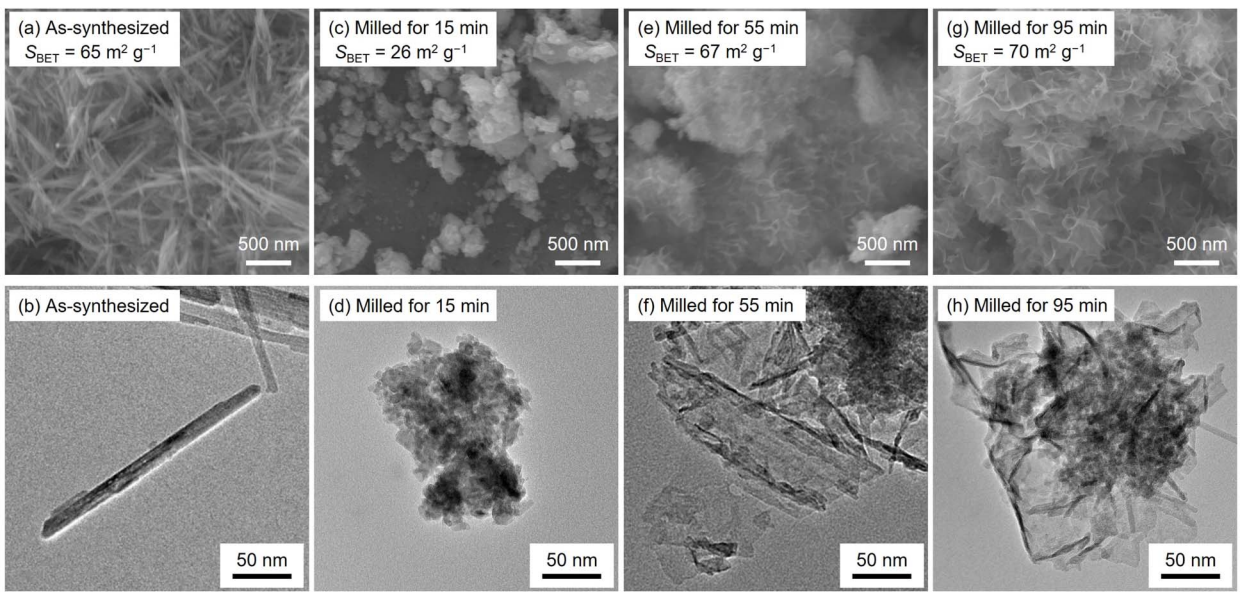

Fig. 2 SEM images, TEM images and specific surface area (S_{BET}) of (a and b) as-synthesized and (c–h) milled samples for different periods.

NO conversion in the wide temperature range due to the lower specific surface area (S_{BET} = 26 m^2 g^{-1}) than that in as-synthesized OMS-2 (S_{BET} = 65 m^2 g^{-1}). Milled OMS-2 for 55 min exhibited 91% of NO conversion at 90 °C, which is the highest value among the tested catalysts in this study. Repeating catalytic test confirmed that milled OMS-2 for 55 min stably worked in the tested temperature range (Fig. 4). Fig. 5(a) shows N_2O evolution over as-synthesized and milled OMS-2 catalysts. All the tested catalysts showed low N_2O evolution as a by-product in the low-temperature region below 90 °C, and the evolution amount of N_2O gradually increased with an increase in reaction temperature, followed by poor N_2 selectivity at high temperatures (Fig. 5(b)). Regarding suppression of N_2O formation, low operating temperature is favored. Thus, milled OMS-2 for 55 min was the best catalyst among the tested catalysts because NO conversion over milled OMS-2 for 55 min reached 100% at a lower temperature range than that of the other tested catalysts and high N_2 selectivity (93% at 90 °C) was also achieved due to the suppression of undesirable N_2O formation by the improved low-temperature activity. The catalytic activity of NH_3-SCR over OMS-2 depends on various factors such as the specific surface area, acidity, redox property, and oxygen vacancies. Except for milled OMS-2 for 15 min, the specific surface areas of the tested samples were almost the same. Therefore, the specific surface areas of the samples did not appear to affect their catalytic activity in this case.

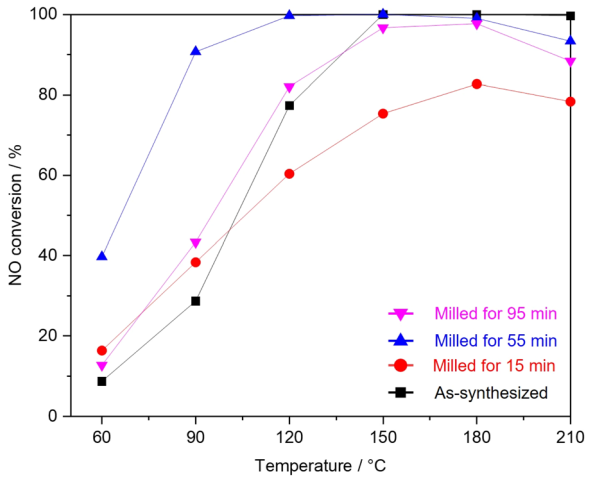

Fig. 3 NO conversion over as-synthesized and milled OMS-2 catalysts.

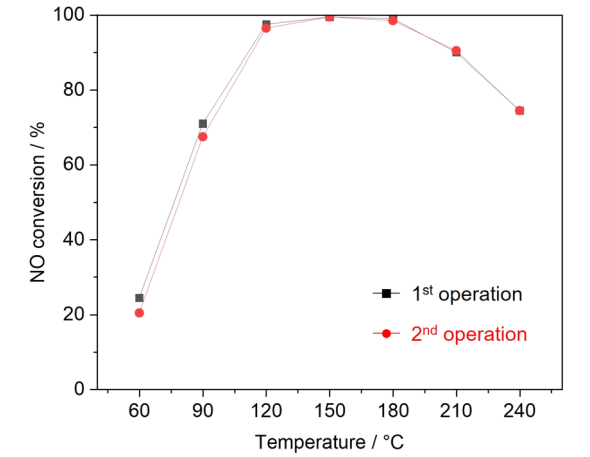

Fig. 4 NO conversion over milled for 55 min in the recycling test. In the recycling test, after the 1st operation, the temperature of the catalyst was cooled down, and then raised again (2nd operation).

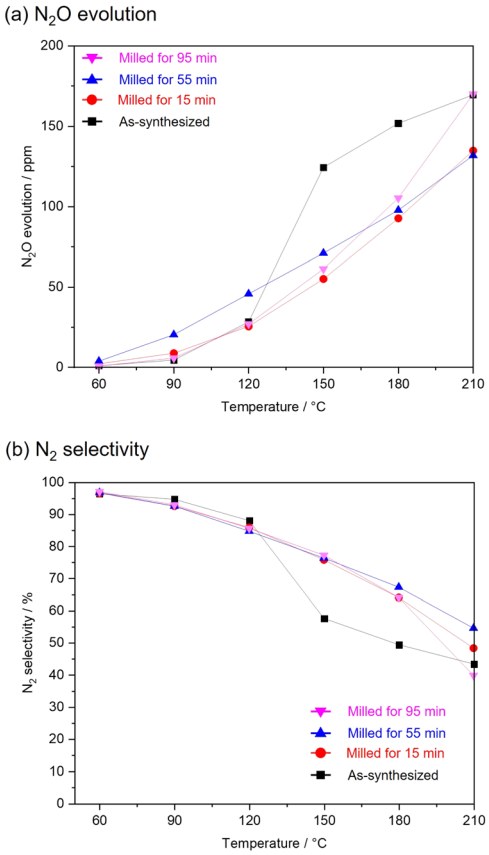

Fig. 5 (a) N_2O evolution and (b) N_2 selectivity over as-synthesized and milled OMS-2 catalysts.

Fig. 6(a) shows XPS spectra of Mn 2p for as-synthesized and milled OMS-2 catalysts. The peak positions in as-synthesized OMS-2 were shifted toward low binding energy after mechanical milling. Mn species contained in metal oxides are generally in a mixed valence state. The peak position of Mn species shifted to low binding energy with the reduction of the valence state of manganese: Mn^{4+} (643.7 eV), Mn^{3+} (641.6 eV) and Mn^{2+} (640.0 eV) in Mn $2p_{3/2}$.[37] Therefore, the peak shift suggests that the average valence of Mn species decreased after the post-synthetic mechanical treatment. In the NH_3-SCR reaction, Mn^{4+} acts as an active center for the dehydrogenation of NH_3.[38] Therefore, the high proportion of Mn^{4+} would be favored to exhibit enhanced NH_3-SCR activity in manganese-based catalysts. XPS analysis revealed that amounts of Mn^{4+} did not increase after the mechanical milling treatment. Thus, at least, there is no positive effect in terms of the valence state of Mn

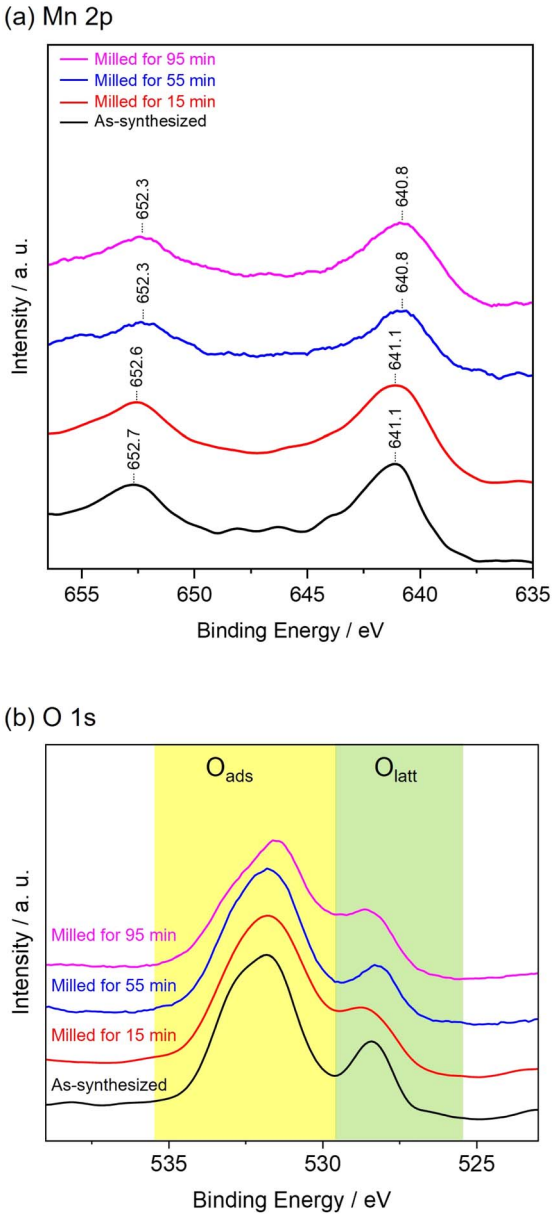

Fig. 6 (a) Mn 2p and (b) O 1s XPS spectra of as-synthesized and milled OMS-2 catalysts.

species. Because the valence state of manganese is known to be +3 in feitknechtite, the peak shift may imply the formation of feitknechtite in the vicinity of the surface of the catalysts.

Fig. 6(b) shows the O 1s for as-synthesized and milled OMS-2 samples. The spectra for O 1s could be divided into two characteristic peaks ascribed to the lattice oxygen species (O_{latt}) at 528.4 eV and adsorbed oxygen species (O_{ads}) at 532.2 eV. O_{ads} species are critical for NH_3-SCR at low temperatures because they have higher mobility than that in the O_{latt} species.[39] Three milled OMS-2 catalysts exhibited higher ratios of O_{ads}/O_{latt} than those of as-synthesized OMS-2 (Table 1), indicating that the planetary ball milling treatment of as-synthesized OMS-2 introduced surface oxygen vacancy defects. In particular, milled OMS-2 for 55 min, showing the best catalytic activity among

Table 1 O_{ads}/O_{latt} and the amount of H_2 consumption of as-synthesized and milled OMS-2 catalysts

Sample	O_{ads}/O_{latt}[a]	H_2 consumption[b]/mmol g^{-1}
As-synthesized	4.2	7.6
Milled for 15 min	5.0	6.5
Milled for 55 min	5.3	5.4
Milled for 95 min	4.6	5.3

[a] Calculated using the ratios of integral peak areas in XPS spectra. [b] Determined using H_2-TPR data.

the tested catalysts, exhibited a highest ratio of O_{ads}/O_{latt}. Even though milled OMS-2 for 15 min also exhibited a higher ratio of O_{ads}/O_{latt} than as-synthesized OMS-2 and milled OMS-2 for 95 min, its NO conversion rates at low temperatures were not high due to its low specific surface area evidenced in Fig. 2(c). Wu *et al.* reported that Ce-doped OMS-2 exhibited enhanced catalytic activity in NH_3-SCR at low temperatures owing to the increased oxygen vacancies.[31] It was deduced that the increased oxygen vacancy defects introduced by planetary ball milling played a critical role to enhance the catalytic activity of the OMS-2 catalyst.

The acidities of the OMS-2 catalysts were analyzed using the NH_3-TPD technique. Fig. 7 shows the NH_3-TPD profiles of the prepared catalysts. The as-synthesized OMS-2 catalyst exhibited two distinct desorption peaks. The desorption peaks at 125 and 275 °C were associated with the weak and strong acid sites, respectively. Although the milled OMS-2 catalysts showed two distinct desorption peaks, the desorption peaks observed for the milled OMS-2 catalysts were located at higher temperatures than those observed for as-synthesized OMS-2 catalyst. This suggests that the milled OMS-2 catalysts have stronger acidic

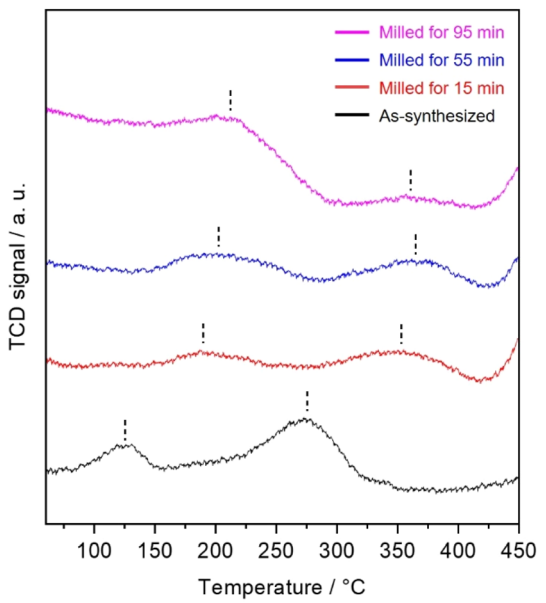

Fig. 7 NH_3-TPD profiles of as-synthesized and milled OMS-2 catalysts.

sites than that in as-synthesized OMS-2. Such surface feature would be also one of the factors that enhances the NH_3-SCR catalytic activity at low temperatures because the enhancement of the acid strength would be beneficial for the adsorption and activation of NH_3.

The H_2-TPR technique was applied to examine the reducibility of the OMS-2 catalysts. Fig. 8 shows the H_2-TPR profiles of the prepared catalysts. The as-synthesized OMS-2 catalyst showed three overlapping peaks at 270, 325, and 344 °C. The peak at 270 °C was ascribed to the reduction of MnO_6-□ (where □ represents oxygen vacancies). The other overlapping peaks represent the reduction of MnO_2 to Mn_2O_3/Mn_3O_4 and then to MnO. In the H_2-TPR profiles of three milled OMS-2 catalysts, new peaks appeared above 350 °C. Decrease in H_2 consumption was also observed in all milled samples compared to the as-synthesized OMS-2 (Table 1). Peak shift toward an increase in temperatures and a decrease in H_2 consumption indicates that the milled OMS-2 catalysts have poorer reducibility than that in the as-synthesized OMS-2 catalyst. Therefore, the planetary ball milling has no positive effect on reducibility in this case. However, as the NH_3-TPD analysis showed, the feitknechtite nanosheets passively acted as adsorption sites with enhanced acidity. The planetary ball milling allowed the OMS-2/feitknechtite heterointerface to form, where OMS-2 and feitknechtite are probably redox sites and NH_3 adsorption sites for the NH_3-SCR reaction, respectively, enhancing the low-temperature NH_3-SCR activity.

As discussed above, post-synthetic treatment for OMS-2 by planetary ball milling allowed to tune structural and physicochemical properties, enhancing the conversion rate at low temperatures. In manganese-based SCR catalysts, metal doping is the latest trend toward the development of catalysts with outstanding low-temperature activity.[29–31,40] However, this contribution using a facile planetary ball milling demonstrated the enhancement of catalytic activity of OMS-2 without metal doping (Table S1†). As a future perspective, further improvement of the NH_3-SCR activity of OMS-2 can be expected with the aid of post-synthetic planetary ball milling and metal doping. Considering that the catalytic activity of the manganese oxide catalyst was improved by the mechanical process, which can be easily scaled up, findings from this study represent a significant advance forward the practical utilization of manganese-based catalysts.

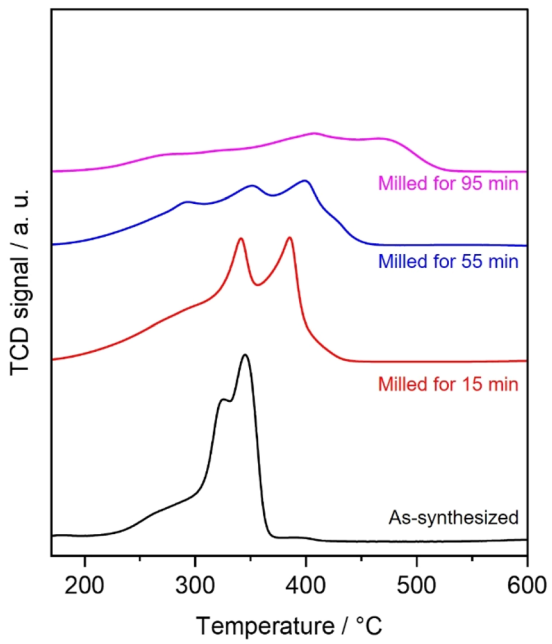

Fig. 8 H_2-TPR profiles of as-synthesized and milled OMS-2 catalysts.

Conclusions

Planetary ball milling was performed on OMS-2 with a nanorod morphology, resulting in a gradual decline in the crystallinity of OMS-2. SEM and HR-TEM observations of the milled OMS-2 samples revealed that feitknechtite with a layered morphology was formed from a part of OMS-2 by the post-synthetic planetary ball milling treatment. The catalytic activity of the as-synthesized and milled OMS-2 samples were compared in the NH_3-SCR reaction. The milled OMS-2 catalyst prepared under the optimum conditions exhibited high NO conversion and high N_2 selectivity at low temperatures. The enhanced low-temperature catalytic activity was probably due to the increased number of oxygen vacancy and enhanced acid strength.

Data availability

The data that support the findings of this study are openly available.

Conflicts of interest

There are no conflicts to declare.

Acknowledgements

This work was supported by New Energy and Industrial Technology Development Organization (NEDO) under Moonshot Project, the Japan Society for the Promotion of Science (JSPS), KAKENHI Grant-in-Aid for Transformative Research Areas (A) JP20A206/20H05880, Grant-in-Aid for Scientific Research (S) JP23H05454 and the Materials Processing Science project ("Materealize") of MEXT, Grant Number JPMXP0219192801.

References

1 K. Skalska, J. S. Miller and S. Ledakowicz, *Sci. Total Environ.*, 2010, **408**, 3976.
2 X. Cheng and X. T. Bi, *Particuology*, 2014, **16**, 1.
3 D. Damma, P. R. Ettireddy, B. M. Reddy and P. G. Smirniotis, *Catalysts*, 2019, **9**, 349.
4 S. Mohan, P. Dinesha and S. Kumar, *Chem. Eng. J.*, 2020, **384**, 123253.
5 L. Han, S. Cai, M. Gao, J. Y. Hasegawa, P. Wang, J. Zhang, L. Shi and D. Zhang, *Chem. Rev.*, 2019, **119**, 10916.

6 H. Li, X. Yi, J. Miao, Y. Chen, J. Chen and J. Wang, *Catalysts*, 2021, **11**, 906.
7 Y. Inomata, H. Kubota, S. Hata, E. Kiyonaga, K. Morita, K. Yoshida, N. Sakaguchi, T. Toyao, K. I. Shimizu, S. Ishikawa, W. Ueda, M. Haruta and T. Murayama, *Nat. Commun.*, 2021, **12**, 557.
8 J. Xiang, X. Du, Y. Wan, Y. Chen, J. Ran and L. Zhang, *Catal. Sci. Technol.*, 2019, **9**, 6085.
9 Y. Wang, T. Nishitoba, Y. Wang, X. Meng, F.-S. Xiao, W. Zhang, B. Marler, H. Gies, D. De Vos, U. Kolb, M. Feyen, R. McGuire, A.-N. Parvulescu, U. Müller and T. Yokoi, *Ind. Eng. Chem. Res.*, 2020, **59**, 7375–7382.
10 Y. Shan, X. Shi, J. Du, Z. Yan, Y. Yu and H. He, *Ind. Eng. Chem. Res.*, 2019, **58**, 5397–5403.
11 L. Liu, Y. Gao, S. Cheng, X. Wu, Y. Ma, X. Zhang, R. Ran, J. Liu, Z. Si, Z. Ren and D. Weng, *J. Environ. Chem. Eng.*, 2022, **10**, 108305.
12 M. Jablonska, *RSC Adv.*, 2022, **12**, 25240.
13 G. Xu, X. Guo, X. Cheng, J. Yu and B. Fang, *Nanoscale*, 2021, **13**, 7052.
14 C. Liu, J.-W. Shi, C. Gao and C. Niu, *Appl. Catal., A*, 2016, **522**, 54.
15 X. Wang, Y. Zheng, Z. Xu, X. Wang and C. Xiaoping, *RSC Adv.*, 2013, **3**, 11539.
16 H. Fan, J. Fan, T. Chang, X. Wang, X. Wang, Y. Huang, Y. Zhang and Z. Shen, *Catal. Sci. Technol.*, 2021, **11**, 6553.
17 T. Uematsu, Y. Miyamoto, Y. Ogasawara, K. Suzuki, K. Yamaguchi and N. Mizuno, *Catal. Sci. Technol.*, 2016, **6**, 222.
18 J. Zhang, B. Dong, Y. Han, X. Zhan, S. Ge and S. He, *Environ. Eng. Res.*, 2022, **28**, 220156.
19 Q. Huang, Z. Zhou, B. Lan, M. Sun, C. Sun and L. Yu, *Colloids Surf., A*, 2023, **666**, 131302.
20 X. Min, M. Guo, K. Li, J. Gu, X. Guo, Y. Xue, J. Liang, S. Hu, J. Jia and T. Sun, *Appl. Surf. Sci.*, 2021, **568**, 150972.
21 S. Zhu, H. Li, L. Wang, Z. Cai, Q. Wang, S. Shen, X. Li and J. Deng, *Chem. Eng. J.*, 2023, **458**, 141415.
22 N. Huang, Z. Qu, C. Dong, Y. Qin and X. Duan, *Appl. Catal., A*, 2018, **560**, 195.
23 B. Zhang, D. Chen, H. Liu, X. Zou and T. Chen, *Aerosol Air Qual. Res.*, 2020, **20**, 1155.
24 Y. Peng, H. Chang, Y. Dai and J. Li, *Procedia Environ. Sci.*, 2013, **18**, 384.
25 F. Zhao, G. Zhang, X. Huang, Z. Tang and F. Zha, *Ind. Eng. Chem. Res.*, 2023, **62**, 9077.
26 J. Guo, F. Gan, Y. Zhao, J. He, B. Wang, T. Gao, X. Jiang and S. Ma, *RSC Adv.*, 2023, **13**, 4032.
27 L. Li, Y. Wang, L. Zhang, Y. Yu and H. He, *Catalysts*, 2020, **10**, 396.
28 Y. Pan, B. Shen, L. Liu, Y. Yao, H. Gao, C. Liang and H. Xu, *Fuel*, 2020, **282**, 118834.
29 X. Wu, X. Yu, Z. Chen, Z. Huang and G. Jing, *Catal. Sci. Technol.*, 2019, **9**, 4108.
30 S. Ming, P. Wang, P. Liu, J. Duan, F. Mei, L. Pang, Z. Chen and T. Li, *Chem. Eng. J.*, 2020, **379**, 122287.
31 X. Wu, X. Yu, X. He and G. Jing, *J. Phys. Chem. C*, 2019, **123**, 10981.
32 T. Kozawa, K. Fukuyama, A. Kondo and M. Naito, *ACS Omega*, 2019, **4**, 5690.
33 A. V. Syugaev, K. A. Yazovskikh, A. A. Shakov, S. F. Lomayeva, A. N. Maratkanova and D. A. Petrov, *Surf. Interfaces*, 2021, **22**, 100816.
34 Y. Yang, S. Zhang, S. Wang, K. Zhang, H. Wang, J. Huang, S. Deng, B. Wang, Y. Wang and G. Yu, *Environ. Sci. Technol.*, 2015, **49**, 4473.
35 K. Yamaguchi, H. Kobayashi, Y. Wang, T. Oishi, Y. Ogasawara and N. Mizuno, *Catal. Sci. Technol.*, 2013, **3**, 318.
36 J. Luo, Q. Zhang and S. L. Suib, *Inorg. Chem.*, 2000, **39**, 741.
37 L. Zhang, D. Zhang, J. Zhang, S. Cai, C. Fang, L. Huang, H. Li, R. Gao and L. Shi, *Nanoscale*, 2013, **5**, 9821.
38 R. T. Guo, B. Qin, L. G. Wei, T. Y. Yin, J. Zhou and W. G. Pan, *Phys. Chem. Chem. Phys.*, 2022, **24**, 6363.
39 T. Boningari, P. R. Ettireddy, A. Somogyvari, Y. Liu, A. Vorontsov, C. A. McDonald and P. G. Smirniotis, *J. Catal.*, 2015, **325**, 145.
40 L. Sun, Q. Cao, B. Hu, J. Li, J. Hao, G. Jing and X. Tang, *Appl. Catal., A*, 2011, **393**, 323.